Advanced Ceramics Progress: Vol. 10, No. 1, (Winter 2024) 34-43

Materials and Energy Research Center
MERC

Contents lists available at ACERP

Advanced Ceramics Progress

Journal Homepage: www.acerp.ir

Original Research Article

Ag/Zn Codoped TiO_2 (AZT) Mesoporous Nanoparticles: Investigation the Optical Properties via Increasing Calcination Temperatures

Negin Ebrahimi [a], Behzad Koozegar Kaleji [b,*]

[a] *Master, Department of Materials Engineering, Faculty of Engineering, Malayer University, Malayer, Iran.*
[b] *Associate Professor, Department of Materials Engineering, Faculty of Engineering, Malayer University, Malayer, Iran.*

* Corresponding Author Email: b.kaleji@malayeru.ac.ir, bkaleji@yahoo.com (B. Koozegar Kaleji) URL: https://www.acerp.ir/article_208070.html

ARTICLE INFO

Article History:
Received: 03 June 2024
Revised: 05 August 2024
Accepted: 19 October 2024

Keywords:
Nanoparticles,
Ag/Zn Codoped TiO_2,
Photocatalytic Activity,
Band Gap,
Calcination Temperature

ABSTRACT

TiO_2 nanoparticles codoped with Ag/Zn (AZT) were prepared using a simple sol-gel method. The effect of calcination temperature on the structural, optical, and photocatalytic properties of nanoparticles synthesized at temperatures of 400, 500, and 600 °C was investigated. The synthesized nanoparticles were analyzed using various methods, including thermal analysis (TG-DTA), X-ray diffraction (XRD), spectrophotometry (UV-Vis), electron microscopy (FESEM & TEM), and surface chemical analysis (XPS). To evaluate the photocatalytic activity of the samples, the degradation of an organic solution of methylene blue (MB) was performed. The results indicated that the calcination temperature significantly affects the microstructure, optical properties, and photocatalytic activity of the samples. The crystal size of AZT nanoparticles was approximately 4.15, 8.13, and 13.6 nm, respectively, with increasing calcination temperature. The optimal condition for the photocatalytic degradation of the methylene blue solution was observed at a calcination temperature of 500 °C, with a degradation percentage of 57.9% under visible light irradiation. Additionally, the bandgap energy of AZT particles decreased from 3.06 eV to 2.25 eV as the calcination temperature increased.

https://doi.org/10.30501/acp.2024.459534.1153

1. INTRODUCTION

Photocatalytic degradation of toxic organic compounds has received significant attention over the past several years. Due to its strong oxidizing power, cost-effectiveness, and long-term stability against photo and chemical corrosion, TiO_2 is widely used in water purification technology (Savio at al., 2016, Kunnamareddy at al., 2021). Today, the photocatalytic degradation of organic compounds is a focus of interest across various industries. Titanium dioxide is one of the most effective semiconductors in this field. One notable feature is its ability to achieve complete organic mineralization under normal conditions, such as ambient temperature and pressure, making it suitable for treating wastewater containing organic pollutants. When charge carriers are available on the semiconductor surface, the holes can produce OH° radicals, which are highly reactive due to the oxidation of OH^- or H_2O. Conversely, electrons can catch molecular oxygen to form a superoxide radical anion $O_2^{\circ -}$, which are also highly reactive (Savio at al., 2016).

TiO_2 exhibits remarkable stability in aqueous environments and is resilient in both acidic and alkaline solutions. It is inexpensive, recyclable, reusable, and relatively simple to produce (Vasiljevic at al., 2020, Mohammad at al., 2019). However, due to the large band

Please cite this article as: Ebrahimi, N. & Koozegar Kaleji, B. (2024). Ag/Zn Codoped TiO2 (AZT) Mesoporous Nanoparticles: Investigation the Optical Properties via Increasing Calcination Temperatures, *Advanced Ceramics Progress*, 10(1), 34-43. https://doi.org/10.30501/acp.2024.459534.1153

gap energy of TiO_2, it primarily absorbs UV light, which constitutes only 3-5% of sunlight and is necessary for photocatalytic activity. Therefore, a photocatalyst activated by visible light that can utilize a larger portion of the solar spectrum is crucial for effective environmental remediation. Several competing effects limit the efficiency of the catalyst (Bellotti at al., 2023). Titanium dioxide (TiO_2) naturally exists in three different crystalline polymorphs: TiO_2 (A: Anatase), TiO_2 (R: Rutile), and TiO_2 (B: Brookite). These polymorphs differ in surface properties, crystal structure, and electronic structure. Anatase tends to transform into rutile at temperatures exceeding 450 °C (Mikrut at al., 2020). Rahmawati et. al. (Rahmawati at al., 2023) concluded that adding silver dopants to the titania structure promotes phase transformation from anatase to rutile and prevents particle growth. Rathi et. al. (Rathi at al., 2023) obtained similar results to Rahmati in their experiments. Kaleji et. al. (Kaleji at al., 2015) investigated the effect of calcination temperature ranging from 350 to 650 °C and concluded that photocatalytic activity increases with rising calcination temperature due to improved phase crystallization (Anatase and Rutile) and a reduction in band gap energy. Lal et. al. (Lal at al., 2021) explored the impact of calcination temperature from 300 to 800 °C on crystalline phases using the sol-gel method. They observed that with increasing calcination temperature, the intensity of anatase peaks decreased while the intensity of rutile peaks increased.

Much research has been done on modifying the physicochemical properties of TiO_2 to shift its absorption threshold to the visible region and separate the photoinduced charges (Rahimi at al., 2023). This can be achieved by coupling it to organic or inorganic dyes (Wang at al., 2016), or by modifying its surface with other semiconductors, doping it with cations, anions, or metals (Anpo at al., 2004), particularly with transition elements such as Ag (Choi at al., 1994), Au (Usha at al., 2016), among others.

Therefore, to obtain the desired photocatalyst, titania must be activated in the visible light range. Research indicates that the addition of impurities to the titania structure significantly affects its properties. The aim of this study is to investigate the effect of calcination temperature on the optical, structural, and photocatalytic properties of titania nanoparticles doped with silver and zinc.

2. MATERIALS AND METHODS

2.1. Raw Materials

Tetrabutyl orthotitanate (TBT = $Ti(OC_4H_9)_4$, purity: 99%), Ethanol (EtOH=C_2H_5OH, purity: 99%), Nitric acid (HNO_3, purity: 65%), Zinc nitrate ($Zn(NO_3)_2$, purity: 99%), and Silver nitrate ($AgNO_3$, purity: 99%) were used in this study. To measure the photocatalytic activity of the samples, methylene blue was used as the color pollutant. All raw materials used in this research were purchased from Merck company with high purity (>98-99%).

2.2. Experimental Procedure

Titania sol was prepared as illustrated in Figure 1. First, 28.8 mL (approximately 0.5 mol) of ethanol was poured into a 100 mL beaker. Then, 3.42 mL (0.01 mol) of the alkoxide precursor (TBT: Tetra n-butyl orthotitanate) was slowly added to the ethanol and stirred for 60 minutes. Next, 0.47 mL (0.0105 mol) of nitric acid (HNO3) was added to the solution. After stirring for 30 minutes, 1.8 mL (0.1 mol) of distilled water was introduced. Following the addition of water, stirring continued for 1-2 hours, and to complete the hydrolysis process, the TiO2 yellow sol was kept at room temperature (25 °C) for 24 hours. Subsequently, the samples were transferred to an oven and dried at 100 °C for 10 hours. The addition of ingredients at each step was carried out slowly and continuously. The samples were calcined at temperatures of 400, 500, and 600 °C in an electric furnace. Following this, two solutions of silver and zinc were added with appropriate content (1 mmol = 0.17 g AgNO3 and 1.5 mmol = 0.3 g Zn(NO3)2) to the TiO2 sol. The prepared solution was stirred on a magnetic stirrer for 1 hour and then dried to form a gel. Finally, the dried gel was placed in the furnace and calcined at different temperatures (400, 500, and 600 °C) to synthesize the desired nanoparticles.

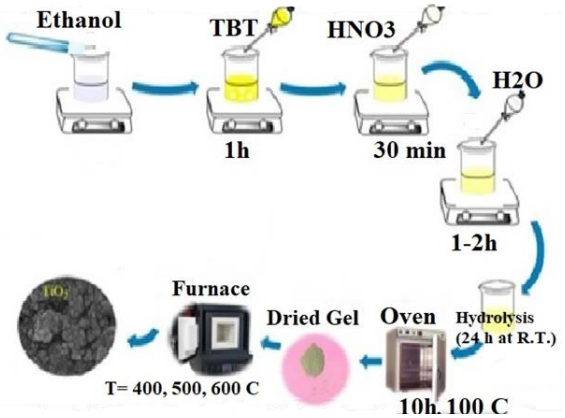

Figure 1. Schematic diagram of preparation of TiO_2 nanoparticles by sol–gel method.

2.3. Nanoparticle Characterization Methods

To check the phase transformation of the jelly sample obtained from titania sol, it was subjected to air atmosphere using TG-DTA analysis with a heating rate of 10 °C/min. The crystal structure and degree of crystallization of the samples were recorded using the MPD-XPERT model XRD machine with a wavelength of λ = 1.54 Å in the angle range of 2θ = 20-80˚, available at Malayer University.

To determine the specific surface area of the synthesized nanoparticles, a BET device (model Belsorp mini II, Japan) was used. The BET system measures the volume of nitrogen gas absorbed and desorbed by the

material surface at a constant temperature of liquid nitrogen (77 K). To investigate the optical properties and calculate the band gap energy of the synthesized samples of titania and titania nanoparticles in the presence of Zn and Ag dopants, a UV-Vis device (model 2000, manufactured by Spekol, Germany) was utilized, also available at Malayer University. X-ray Photoelectron Spectroscopy (XPS) was recorded by a PHI 5000C spectrometer using MgKα radiation (hυ = 1253.6 eV). The reference peak for calibrating the device was C1s at 284.6 eV.

Field Emission Scanning Electron Microscope (FE-SEM), MIRA3-TESCAN (10-15 kV) model, and Transmission Electron Microscopy (TEM: Philips EM208, 100 kV) were used to examine the morphology.

2.4 Photocatalytic Activity

In this research, the photocatalytic test involved the degradation of methylene blue solution with a concentration of 10 ppm in the presence of synthesized nanoparticles. To determine the amount of absorption, 0.1 g of the synthesized powder was added to the methylene blue solution, and the light absorption was measured at different time intervals under visible light radiation at a wavelength of 664 nm (the maximum absorption for methylene blue) using a spectrophotometric device. The irradiation time for the synthesized samples was set at 1 hour, with intervals of 15, 30, 45, and 60 minutes. Using Equation (1), the degradation percentage of pollutant was calculated based on the absorption peaks (Zou at al., 2017).

$$\eta(\%) = (1 - A_t/A_0) \times 100 \quad (1)$$

In this relation, A_0 represents the initial absorption without radiation in the dark environment (t = 10 min at dark place), and A_t the absorption of methylene blue solution after irradiation in different time intervals. Spectrophotometer data was used to obtain the A_t value. To measure the band gap energy of the synthesized samples in this research, first, 0.01 g of the synthesized powder was ultrasonicated with 8 ml of EtOH and 2 ml of HNO_3 for 1-2 hours and then, all samples were irradiated. Visible light UV-VIS spectroscopic analysis was also performed.

The optical band gap energy (E_g) of the samples was calculated using the relationships and previous research (Ahmadi at al., 2021), as summarized in the following formula:

$$E_g\ (eV) = 1240/\lambda_{edge} \quad (2)$$

where λ_{edge} represents the absorption limit of the semiconductor obtained from the UV-Vis spectrophotometric results.

3. RESULTS AND DISCUSSION

3.1. TG-DTA analysis

In Figure 2, the differential thermal analysis curve of pure titania gel is presented.

An endothermic peak is observed in the temperature range of 0 to 135 °C, which is associated with the release of ethanol solvent, water, and volatile substances in the raw materials (8.66 wt%). An exothermic peak occurs in the temperature range of 375 to 425 °C, corresponding to the maximum crystallization temperature of the anatase phase at 395 °C. Another exothermic peak appears in the temperature range of 520 to 580 °C, related to the transformation of the anatase phase to rutile (500 °C) (Choi at al., 1994). The second stage of weight loss, which occurs at temperatures above 135 °C and accounts for about 10%, is associated with the removal of structural water and the phase transformation of titanium hydroxide to titanium dioxide. The weight change curve at temperatures above 600 °C remains almost constant, indicating the complete removal of water and other organic compounds, with a total weight loss of 15.88%. Based on the results of thermal analysis, the temperature range of 400 to 600 °C has been selected for the calcination process of the samples.

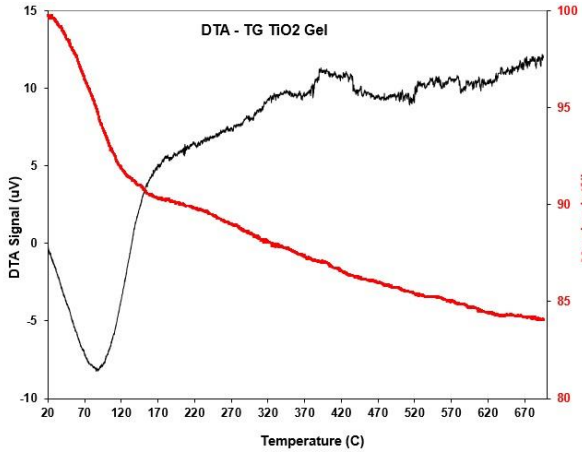

Figure 2. TG-DTA curve titania precursor gel.

3.2. XRD Analysis

The phase analysis of pure (T) and doped samples (AT, ZT, AZT) calcined at 400 °C is given in Figure 3a. All peaks at this temperature across all samples are attributed to the anatase phase with reference code 21-1272, observed at the angles (2θ) of 25.45, 37.5, 47.7, 54.26, 55.62, and 62.97, respectively. These angles align with the Miller indices (101), (112), (200), (105), (211), and (204), respectively. In the doped samples, the partial shift of the (101) plane to lower angles (Figure 3b) is observed, attributed to the larger ionic radius of the dopant elements (Ag^{+}-Zn^{2+}) compared to the matrix phase (Ti^{4+}). This peak shift was greater in the codoped sample (AZT400), as shown in Figure 3b.

Figure 3a shows no trace of the oxide peaks from Ag_2O and ZnO metal cations, nor from Zn^{2+} and Ag^{+} cations in any of the samples. This absence indicates the successful replacement of metal cations within the titania lattice. The addition of dopants increases the distance between plates (d(hkl)), broadens the peak widths (β), and decreases their intensity, all of which provide evidence for the presence of dopants in the titania lattice, suggesting finer grains. The crystallite sizes of the T, AT, ZT, and AZT samples calcined at 400 °C are 9.15, 8.87, 7.72, and 4.15 nm, respectively. Furthermore, the addition of transition metals to the structure of titania nanoparticles inhibits the phase transformation from anatase to rutile (Lal at al., 2021).

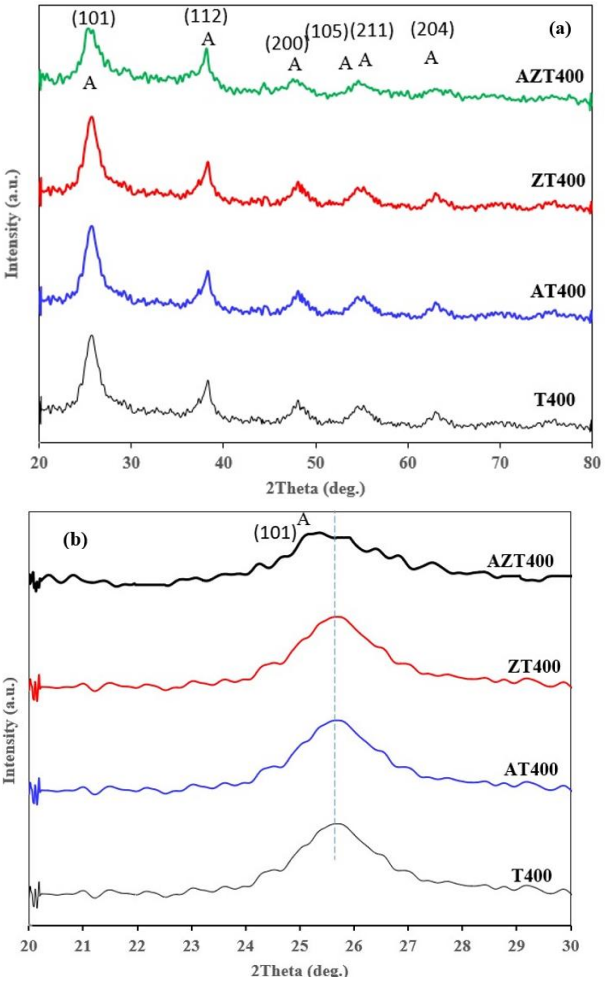

Figure 3. a) XRD patterns of pure sample (T400) and codoped TiO_2 mesoporous nanoparticles (AT, ZT, AZT) calcined at 400 °C for 1 h, b) shift (101) peak with details.

The XRD results of the doped sample at different temperatures (400, 500 and 600 °C) are reported in Figure 4. As the calcination temperature increases, the intensity of the peaks in all samples also increases, indicating a rise in the crystallinity of the structures. Conversely, with increasing temperature, there is a higher percentage of the rutile phase compared to the anatase phase. The percentage of phases and the crystallite sizes of the samples are reported in Table 1.

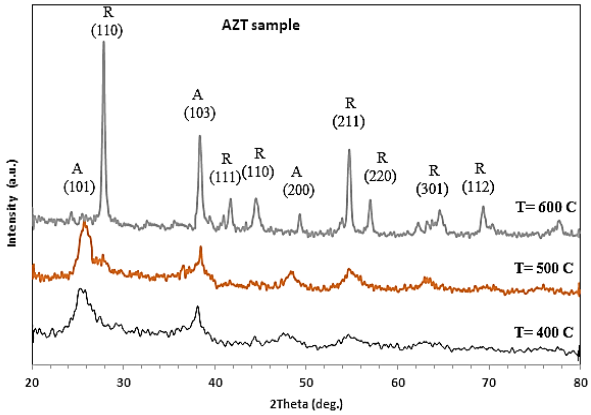

Figure 4. XRD samples of Ag/Zn codoped TiO_2 (AZT) mesoporous nanoparticles calcined at different Temperatures.

TABLE 1. Physical properties of doped samples synthesized at different temperatures.

Samples	Crystallite size (nm)	A (%)	R (%)	BET (m^2/g)
AZT400	4.15	100	-	133.8
AZT500	8.13	86	14	49.5
AZT600	13.6	7	93	6.4

According to Table 1, the crystallite size of AZT400 is equal to 4.15 nm. At a temperature of 400 °C, we observed 10% of the anatase phase; as the temperature increased, the percentage of the rutile phase also increased. At 500 °C, there is 86% anatase and 14% rutile, calculated using the following formula (Eq. 3). At 600 °C, the percentage of the rutile phase has increased to 93%. The crystallite sizes of the samples at 500 °C and 600 °C are 8.13 nm and 13.6 nm, respectively. The percentage of the rutile phase in the sample is calculated using the following equation (Choi at al., 1994)

$$X_R = (1+0.8I_A/I_R)^{-1} \quad (3)$$

where, X_R represents the weight percentage of rutile phase while I_A and I_R denote the peak intensity at diffraction angles of 25.4 corresponding to the (101) plane of the anatase phase and 27.3 corresponding to the (110) plane of the rutile phase.

3.3. Optical Analysis

The results of UV-Vis spectrophotometric analysis of AZT samples calcined at different temperatures (400, 500, 600 °C) are shown in Figure 5. The highest amount (57.9%) of photocatalytic degradation corresponds to the sample synthesized at 500 °C. According to the phase analysis of the AZT calcined at 500 °C, we can see that it consists of two phases, anatase and rutile, with a higher percentage of the anatase phase compared to the rutile phase (Table 1). According to some research, a

combination that includes both anatase and rutile phases, with a higher percentage of the anatase phase relative to the rutile phase, demonstrates better photocatalytic activity (Usha at al., 2016).

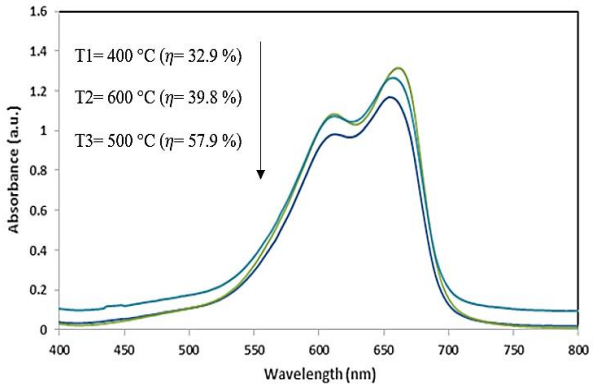

Figure 5. UV-Vis analysis of MB solution in the presence of AZT at different temperatures during 1h under visible light irradiation.

In fact, the main factor contributing to the separation of electrons and holes is the presence of the rutile phase in the structure alongside the anatase phase (Zou at al., 2017). Excited electrons in the rutile phase move to the conduction band of the anatase phase, creating a hole in the valence band of the rutile phase, thereby reducing electron-hole recombination (Ahmadi at al., 2021). Generally, the mixture of the two phases, anatase and rutile, facilitates the transfer of electrons from the anatase phase to the rutile phase (which has a lower energy level). This transfer reduces the rate of recombination in the catalysts of the two-phase mixture and improves electron-hole separation, leading to increased photocatalytic activity. Additionally, the sample calcined at 600 °C exhibits the highest degradation after the sample calcined at 500 °C, which can be attributed to the greater crystallization of the structure.

The proposed mechanism in this research for the photocatalytic process is as follows: TiO_2 is an optically active semiconductor. When it is exposed to light with an energy equal to or greater than its band gap energy (E_g), electrons are excited from the Valence Band (VB) to the Conduction Band (CB), thus creating positive holes (h^+) at the valence level. TiO_2 nanoparticles doped with Ag can indirectly change the charge transfer process on the surface and act as an effective electron acceptor. Reduction in the electron-hole pair recombination can lead to photocatalytic activity. Ag fermi level is lower than TiO_2 conduction band, and electrons can easily transfer from TiO_2 conduction band to Ag. Therefore, it is possible to form a Schottky barrier in the contact area of Ag and TiO_2. Like Ag, Zn cation has a lower fermi level than TiO_2, thus enabling it to trap the excited electrons. As a result, the presence of a small amount of metal in contact with the photocatalyst can trap the generated electrons (e^-) and holes (h^+) and prevent their recombination. Given that Ag and Zn fermi level is lower than TiO_2, electrons can be easily transferred from TiO_2 to Ag and Zn. In this case, it is not possible to recombine these electrons with holes created on the surface of TiO_2. Consequently, more holes areformed on the surface and participate in oxidation reactions - OH and H_2O to hydroxyl radicals. Hydroxyl radicals have a high oxidation potential to destroy the pollutants and turn them into CO_2 and H_2O.

The BET-BJH analysis of the nanoparticles was also conducted. All the calcined samples (AZT400, AZT500, AZT600) exhibit a mesoporous structure, which is most pronounced in the AZT500 sample (Figure 6). The BET surface areas (m^2/g) of the nanoparticles at calcination temperatures of 400, 500, and 600 °C are approximately 133, 49, and 6 m^2/g, respectively. The results of this analysis for the AZT samples at three temperatures 400, 500, and 600 °C are reported in Table 1. The hysteresis loop for this sample is classified as type IV according to the IUPAC standard (Gorgani at al., 2020, Dinkar at al., 2016), and the absorption-desorption curve indicates that this sample possesses a mesoporous structure. The average pore diameter in the AZT500 sample is 8.3 nm (Fig- 6b).

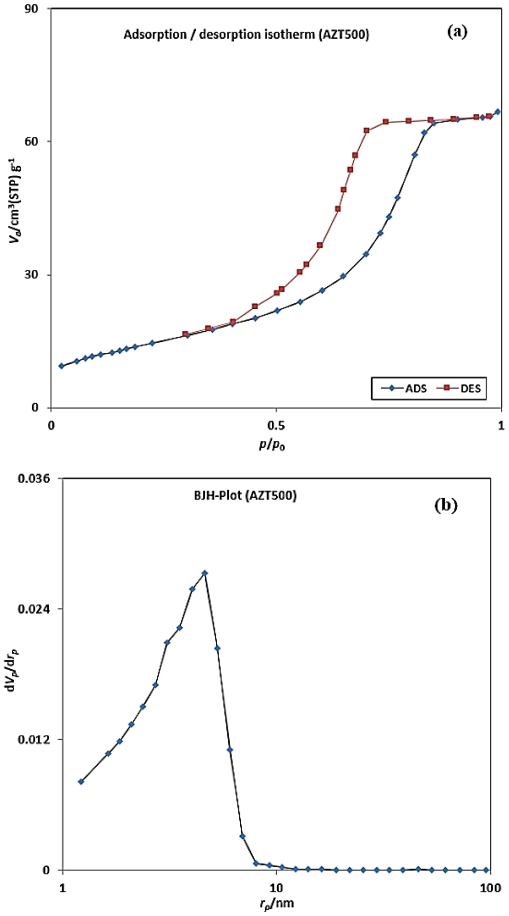

Figure 6. N2 physisorption isotherms (BET) of AZT500 mesoporous nanoparticles calcined at 500 °C. a) BET, b) BJH.

The results of the band gap energy (Eg) of the sample, along with the valence band energy (EVB) and conduction band energy (EcB) of pure and codoped TiO2 samples at temperatures of 400, 500, and 600 °C, are reported in Table 2. Typically, the absorption spectrum of the AZT500 sample, shown in Figure 7, is reported to calculate the band gap energy using Formula 2.

Using the optical band gap energy (Eg) results of the samples and the equations below (Eq. 4 and 5), the valence band energy and conduction band energy of the samples were calculated and reported in Table 2.

$$E_{VB} = X - E_e - 0.5 \times E_g \quad (4)$$

$$E_{CB} = E_{VB} - E_g \quad (5)$$

where E_{VB} is the valance band edge potential, X the electronegativity of the semiconductor which is the geometric mean of the electronegativity of the constituent atoms (X of TiO_2 is 5.81 eV), E_e the free electron energy in the hydrogen scale (4.5 eV) (Gupta at al. 2012, Khan at al., 2017), and E_g the optical band gap.

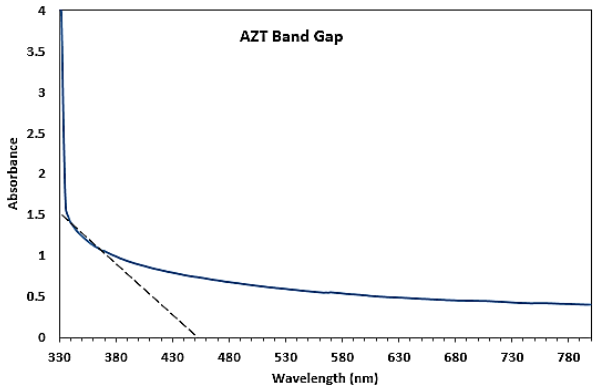

Figure 7. UV-Vis spectra of AZT500.

TABLE 2. Optical properties of synthesized samples at different temperatures

Sample	Eg (eV)	VB (eV)	CB (eV)
T400	3.22	2.92	- 0.3
T500	2.88	2.75	- 0.13
T600	2.83	2.73	- 0.105
AZT400	3.06	2.84	- 0.217
AZT500	2.75	2.69	- 0.062
AZT600	2.25	2.44	- 0.109

3.4. XPS Analysis of AZT-500 sample

The chemical states of the elements in T500 and AZT500 samples were analyzed based on the XPS analysis, the results of which are given in Figure 8. Figure 8a is the broad spectrum of pure titania sample (T500). As shown in Figure 8a, the presence of Ti and O elements indicates the presence of pure titania in the composition. Additionally, a wide scan of the doped sample (AZT500) is shown in Figure 8b. The presence of Ag and Zn cations indicates the doping of these cations in the titania structure. For further investigation, higher resolution spectra of the samples were obtained. The high-resolution Ti 2p spectrum of the AZT500 sample is shown in Fig.8c. Two peaks are observed around the binding energies of 458.3 eV and 464.3 eV, which correspond to Ti 2p3/2 and Ti 2p1/2, respectively. The binding energy difference between these two peaks is about 6 eV, confirming the presence of the Ti element in the form of Ti^{4+} (Dinkar at al., 2016). Figure 8d displays the high-resolution Ag 3d spectrum of the AZT500 sample. The two peaks identified at binding energies of 372.1 eV and 378.8 eV are related to Ag 3d5/2 and Ag 3d3/2. There is an energy difference of 6.7 eV between the binding energies of the Ag peaks, indicating that Ag is in the Ag0 state on the TiO_2 lattice (Khan at al., 2017). Figure 8e Figure 8e shows two peaks related to the presence of Zn cations at binding energies of 1021.9 eV and 1045.7 eV, corresponding to Zn 2p3/2 and Zn 2p1/2. The difference in binding energy between these two peaks is 23.8 eV, indicating the presence of Zn2+ ions in the sample (Choi at al., 1994). The XPS spectrum of the O1s level (Figure 8f) is indicative of a chemical state for oxygen. The lattice oxygen in the crystal (O_L) of TiO_2 is approximately 530.5 eV. The O 1s spectrum can be split into two types of oxygen species: (I) the binding energy at 530.5 eV, which is associated with the lattice oxygen (O_L); and (II) the 531.4 eV peak, which is assigned to the hydroxyl groups (OH) (Ana at al. 2023, Ghotbi at al., 2020, Kingsley at al., 2021).

3.5. Morphological Analysis

FESEM analyses have been used to investigate the morphology of pure and doped titania nanoparticles. From the optimal photocatalytic conditions (AZT500), FESEM images and elemental analysis (EDS) have been obtained, as shown in Figures 9. As depicted in the images (Figure 9a), the nanoparticles are largely agglomerated, with a particle size range of 25-50 nm for the pure sample (T500, Figure 9a) and 15-30 nm for the doped sample (T500, Figure 9a) and 15-30 nm for the doped sample (AZT500, Figure 9b). The elemental analysis (EDS) of the samples confirmed the presence of titanium and oxygen elements in the pure sample (Figure 9c) as well as the presence of titanium, oxygen, zinc, and silver elements in the doped sample (AZT500, Figure 9d).

To accurately check the size of the particles, the analysis of transmission electron microscope images was carried out. TEM images of the sample calcined at 500 °C with the best photocatalytic conditions are shown in Figure 10. The particle size distribution is in the range of 10-20 nm (Figure 10a). The interplanar spacing was estimated using HRTEM images (Figure 10b), obtaining values of 0.351 nm and 0.335 for the anatase and rutile phase.

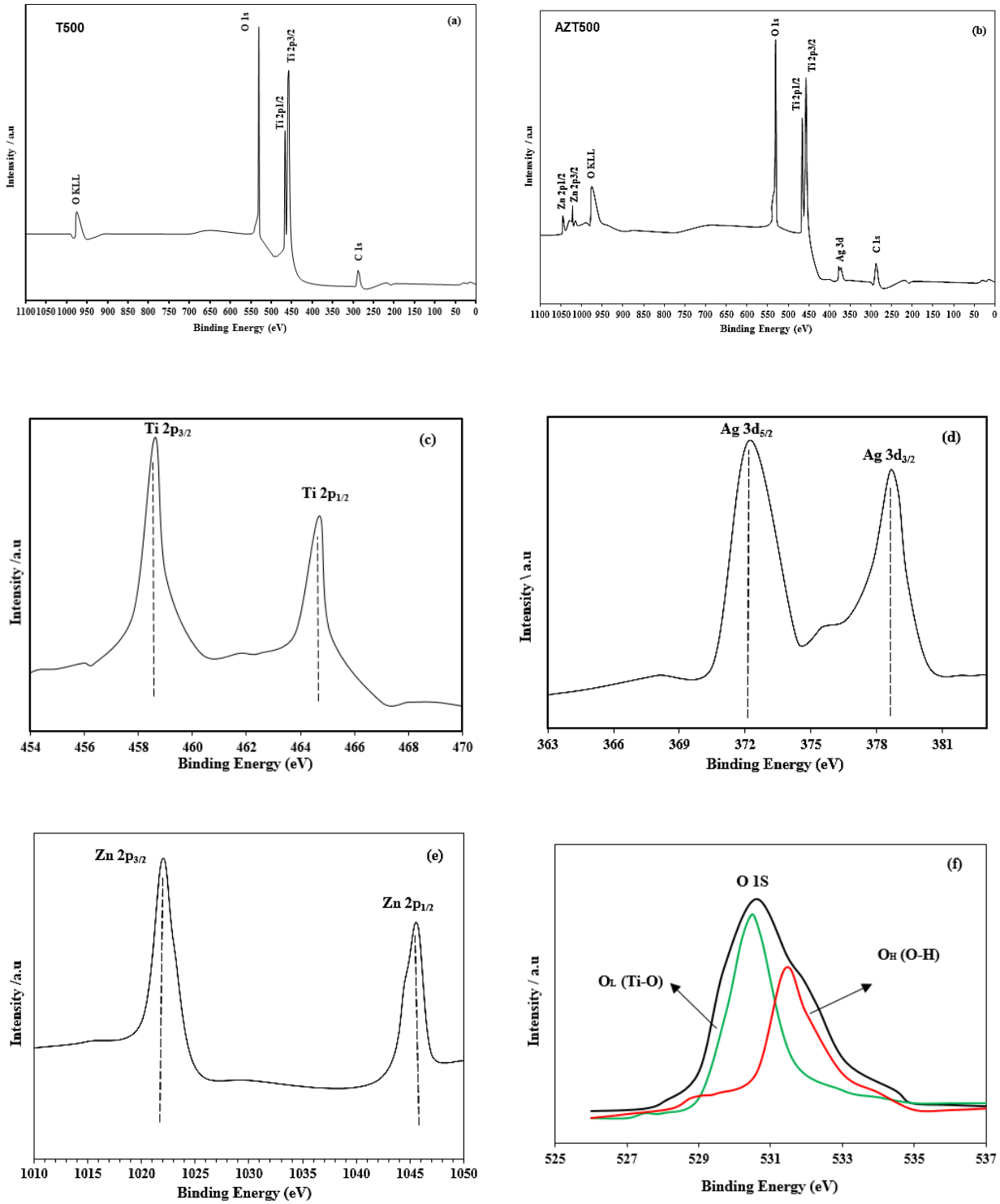

Figure 8. XPS spectra (a) wide scan of pure TiO_2 nanoparticles (T500), (b) codoped TiO_2 nanoparticles (AZT500) calcined at 500 °C, (c) Ti2p region (d), Ag 3d region, (e) Zn 2p region and (f) O 1s region.

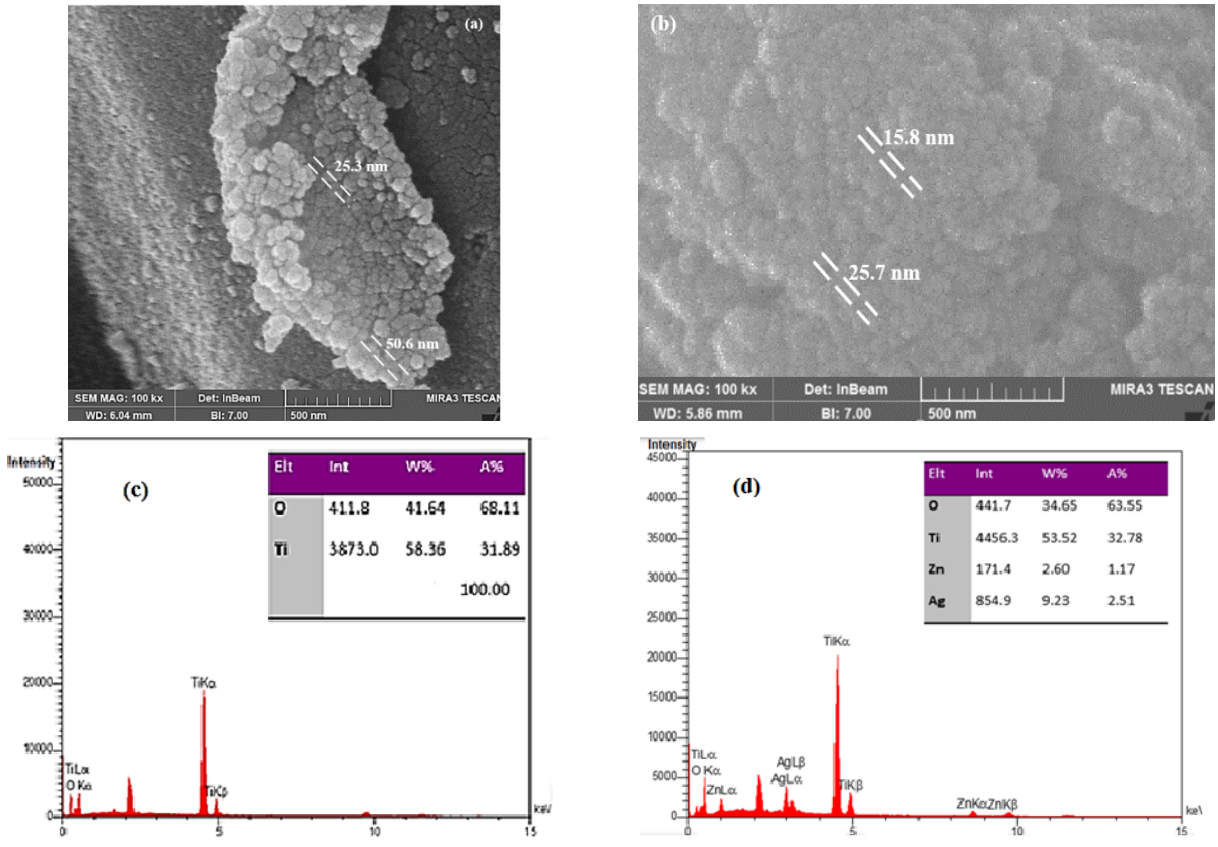

Figure 9. FESEM-EDS images of undoped TiO_2 (**a, c**) and codoped (AZT) sample (**b, d**) calcined at 500 °C.

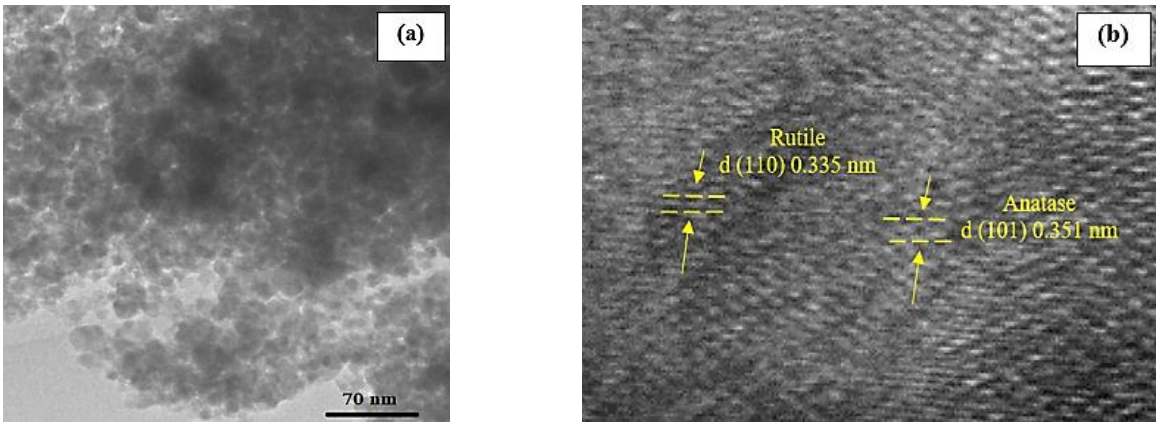

Figure 10. The TEM (a) and HRTEM (b) images of an AZT500 nanoparticles.

Briefly, one of the parameters affecting the photocatalytic activity of the samples is the surface area of the particles, which, in turn, depends on their morphology (spherical, needle-shaped, rod-shaped, amorphous, etc.). Considering that nanoparticles with dimensions less than 25 nm were obtained during the synthesis process, it is expected that these particles will exhibit better photocatalytic properties. Based on the results from Figure 9 and Figure 10, the synthesized particles have an almost spherical shape. According to the BET results (Table 1), they are suitable for photocatalytic activity due to their high specific surface area. To study the effects of morphology and other parameters such as specific surface area on photocatalytic activity, both the as-grown and air-annealed nanostructures were tested for methylene blue (MB) degradation under Visible light. Of note, the morphology of a sample affects the optical properties. The significance of morphology control depends not only on modifications of the band gap (Table 2) but also on the efficiency of the photocatalytic process. The crystallinity, porosity, and morphology of a sample are closely related to the synthesis methodology, which is

why it is necessary to find a method that allows for the control of these properties.

4. CONCLUSION

In this research, TiO_2 nanoparticles codoped with Ag and Zn were prepared using the sol-gel method. The results are as follows:

- By incorporating Ag and Zn cations into the of titania nanoparticles, the crystalline particle size is reduced, and the phase transformation from anatase to rutile is prevented. In other words, the doping of these two cations in the titania lattice acts as a stabilizer for the anatase phase.
- Increasing the calcination temperature of the AZT samples led to a decrease in specific surface area, which reached 133.8 m^2/g at 400 °C and 49.5 m^2/g at 500 °C. This increase in temperature also caused the particle size to grow from 4.15 nm to 8.13 nm.
- The best photocatalytic properties were observed in the AZT sample calcined at 500 °C, where its degradation percentage was 57.9%.
- An increase in calcination temperature from 400 °C to 600 °C resulted in a decrease in band gap energy from 3.06 eV to 2.25 eV.
- The results from FESEM analysis showed that the particle size of the synthesized sample at the optimal photocatalytic degradation temperature (500 °C) was smaller than that of the undoped TiO_2 sample. The particle size range for the undoped TiO_2 (T500) sample was approximately 25–50 nm, while the range for the AZT500 sample was about 15–30 nm.

ACKNOWLEDGMENTS

This study was funded by Malayer University. The authors highly acknowledge the financial support of Malayer University.

REFERENCES

1. Ahmadi, M. & Koozegar Kaleji B. (2021). TCA (Ag doped TiO_2-CuO) mesoporous composite nanoparticles: optical, XPS and morphological characterization, *Journal of Materials Science, Materials in Electronic*, *32*, 13450-13461. https://doi.org/10.1007/s10854-021-05923-5

2. Anpo, M. (2004). Preparation characterization, and reactivities of highly functional titanium oxide-based photocatalysts able to operate under UV–visible light irradiation: approaches in realizing high efficiency in the use of visible light. *Bulletin of the Chemical Society of Japan*, *77*, 1427–1442. https://doi.org/10.1246/bcsj.77.1427

3. Ana E. Cardozo, Elsa M. Farfán Tores, Graciela V. Morales, Edgardo L. Sham (2023) Sol–gel synthesis of TiO_2 doped with chromium: photocatalytic degradation of tartrazine, *Academia Materials Science*, *1*, 1-9. https://doi.org/10.20935/AcadMatSci6142

4. Bellotti, V., Daldossi, C., Perilli, D., D'Arienzo, M., Stredansky, M., Di Valentin, C., & Simonutti, R. (2023). Mechanism of sustainable photocatalysis based on doped-titanium dioxide nanoparticles for UV to visible light induced PET-RAFT photo-polymerization. *Journal of Catalysis*, *428*, 115074. https://doi.org/10.1016/j.jcat.2023.07.015

5. Choi, W., Termin, A. & Hoffmann, M.R. (1994). The role of metal ion dopants in quantum-sized TiO_2: correlation between photoreactivity and charge carrier recombination dynamics. *Journal of Physical Chemistry. 98*, 13669–79. http://dx.doi.org/10.1021/j100102a038

6. Aware, D. V. & Jadhav, S. S. (2016). Synthesis, characterization and photocatalytic applications of Zn-doped TiO_2 nanoparticles by sol–gel method, *Applied Nanoscience*, 6, 965–972. https://doi.org/10.1007/s13204-015-0513-8

7. Gupta, S. & Tripathi, M. (2012). A review on the synthesis of TiO_2 nanoparticles by solution route, *Open Chemistry., 10 (2)*, 279–294. https://doi.org /10.2478/s11532-011-0155-y

8. Ghotbi M.Y., Javanmard A. & Soleimani H. (2020). A casting strategy to produce 3D bulk monolithic carbon and N-doped carbon nanosheets with high surface area and low volume, *Microporous and Mesoporous Materials*, *293*, 109791. https://doi.org/10.1016/j.micromeso.2019.109791

9. Gorgani M. & Koozegar Kaleji B. (2020). Structural, photocatalytic and surface analysis of Nb/Ag codoped TiO_2 mesoporous nanoparticles, *Journal of Sol-Gel Science and Technology*, *96*, 728–741. https://doi.org/10.1080/03067319.2020.1767096

10. Ilkhechi, N.N., Ahmadi, A., & Koozegar Kaleji, B. (2015). Optical and structural properties of nanocrystalline anatase powders doped by Zr, Si and Cu at high temperature, *Optical Quantum Electronic*, *47(8).* 2423–2434. https://doi.org/ 10.1007/s11082-015-0120-7

11. Khan, S., Cho, H., Kim, D., Han, S.S., Lee, S.H. K.W., Cho, S.H., Song, T. & Choi, H. (2017). Defect engineering toward strong photocatalysis of Nb-doped anatase TiO_2: Computational predictions and experimental verifications, *Applied. Catalyst B Environmental*, *206*, 520–530. https://doi.org/10.1016/j.apcatb.2017.01.039

12. Egbo, K. O., Shil, S. K., Kwok, C. G., Wang, Y., Liu, C. P., & Yu, K. M. (2021). Band alignment of wide bandgap NiO/MoO3 and NiO/WO3 pn heterojunctions studied by high-resolution X-ray photoelectron spectroscopy. *Journal of Alloys and Compounds*, *876*, 160136. https://doi.org/10.1016/j.jallcom.2021.160136

13. Kunnamareddy, M., Rajendran, R., Sivagnanam, M., Rajendran, R., & Diravidamani, B. (2021). Nickel and sulfur codoped TiO 2 nanoparticles for efficient visible light photocatalytic activity. *Journal of Inorganic and Organometallic Polymers and Materials*, *31*, 2615-2626. https://doi.org/10.1007/s10904-021-01914-5

14. Lal, M., Sharma, P., & Ram, C. (2021). Calcination temperature effect on titanium oxide (TiO2) nanoparticles synthesis. *Optik*, *241*, 166934.\. https://doi.org/10.1016/j.ijleo.2021.166934

15. Mikrut, P., Kobielusz, M., Indyka, P., & Macyk, W. (2020). Photocatalytic activity of TiO2 polymorph B revisited: physical, redox, spectroscopic, and photochemical properties of TiO2 (B)/anatase series of titanium dioxide materials. *Materials Today Sustainability*, *10*, 100052. https://doi.org/10.1016/j.mtsust.2020.100052

16. Mohammad, M. R., Ahmed, D. S., & Mohammed, M. K. (2019). Synthesis of Ag-doped TiO 2 nanoparticles coated with carbon nanotubes by the sol–gel method and their antibacterial activities. *Journal of Sol-Gel Science and Technology*, *90*, 498-509. https://doi.org/ 10.1007/s10971-019-04973-w

17. Rahmawati, T., Butburee, T., Sangkhun, W., Wutikhun, T., Padchasri, J., Kidkhunthod, P., ... & Sapcharoenkun, C. (2023). Green synthesis of Ag-TiO2 nanoparticles using turmeric extract and its enhanced photocatalytic activity under visible light. Colloids and Surfaces A: *Physicochemical and Engineering Aspects*, *665*, 131206. https://doi.org/10.1016/j.colsurfa.2023.131206

18. Rahimi, S., Koozegar Kaleji, B., & Kazazi, M. (2023). ZnxCo3-xO4 Hydrothermally Mesoporous Nanoparticles (ZCH): Structure, Optical, and Surface Analysis. *Advanced Ceramics Progress, 9(1)*, 28-37. https://doi.org/10.30501/acp.2023.379335.1115

19. Rathi, V. H., Jeice, A. R., & Jayakumar, K. (2023). Green synthesis of Ag/CuO and Ag/TiO2 nanoparticles for enhanced photocatalytic dye degradation, antibacterial, and antifungal properties. *Applied Surface Science Advances*, *18*, 100476. https://doi.org/10.1016/j.apsadv.2023.100476

20. Savio, A. K. P. D., Fletcher, J., Smith, K., Iyer, R., Bao, J. M., & Hernández, F. R. (2016). Environmentally effective photocatalyst CoO–TiO2 synthesized by thermal precipitation of Co in amorphous TiO2. *Applied Catalysis B: Environmental*, *182*, 449-455. https://doi.org/ 10.1016/j.apcatb.2015.09.047

21. Usha, K., Kumbhakar, P., & Mondal, B. (2016). Effect of Ag-doped TiO2 thin film passive layers on the performance of photo-anodes for dye-sensitized solar cells. *Materials Science in Semiconductor Processing*, *43*, 17-24. https://doi.org/10.1016/j.mssp.2015.11.015

22. Vasiljevic, Z. Z., Dojcinovic, M. P., Vujancevic, J. D., Jankovic-Castvan, I., Ognjanovic, M., Tadic, N. B., ... & Nikolic, M. V. (2020). Photocatalytic degradation of methylene blue under natural sunlight using iron titanate nanoparticles prepared by a modified sol–gel method. *Royal Society open science*, *7(9)*, 200708. https://doi.org/10.6084/m9.figshare.c.5105934.

23. Wang, D., Leng, Z., Hüben, M., Oeser, M., & Steinauer, B. (2016). Photocatalytic pavements with epoxy-bonded TiO2-containing spreading material. *Construction and building materials*, *107*, 44-51. https://doi.org/10.1016/j.conbuildmat.2015.12.164

24. Zou, Z., Zhou, Z., Wang, H., & Yang, Z. (2017). Effect of Au clustering on ferromagnetism in Au doped TiO2 films: theory and experiments investigation. *Journal of Physics and Chemistry of Solids*, *100*, 71-77. https://doi.org/10.1016/j.jpcs.2016.09.011